Large Deflections of Clamped Circular Plates Under Initial Tension and Transitions to Membrane Behavior

Mark Sheplak*
Microsystems Technology Laboratories
Massachusetts Institute of Technology
Room 39-561
77 Massachusetts Avenue
Cambridge, MA 02139

John Dugundji
Technology Laboratory for Advanced Composites
Department of Aeronautics and Astronautics
Massachusetts Institute of Technology
Room 9-468
77 Massachusetts Avenue
Cambridge, MA 02139

To appear in *Journal of Applied Mechanics*

Abstract

The large deflections of a clamped, circular plate are investigated over a wide range of transverse loadings and initial in-plane tension loads. The continuous transition from plate behavior to membrane behavior is described in detail, along with the development of the accompanying edge zone region where properties change rapidly. We give a simple approximation of this edge zone and its properties, provide limits for the validity of small deflection, linear theory, and note the similar effects of large in-plane tension and large transverse loading. The values and trends are presented in general non-dimensional form, and should prove useful for the design of thin circular disks for micro-sensing applications.

*Member ASME.

1 Introduction

Recently, there has been considerable interest in using thin films of silicon-based materials in miniature mechanical devices and components (for example, Sze 1994). Silicon micromachining processes, prevalent in the microelectronics industry, permit the miniaturization of sensors for the measurement of pressure, temperature, and other physical, electrical and chemical quantities (Sze, 1994). One such application deals with the development of very small silicon pressure sensors for measuring both static and dynamic pressure (Clark and Wise, 1979 and Schellin and Hess, 1992). Often these devices involve small, very thin films (≈ 3000Å) under initial membrane tension (Löfdahl *et al.*, 1994). The tension present in these films can be as large as 1 GPa (Cho *et al.*, 1992). Unfortunately, scaling arguments indicate that the deflection-based pressure sensitivity of such films is expected to degrade significantly (Chau and Wise, 1987). These arguments, however, were made without study of how initial tension affects the onset of nonlinearity. Furthermore, little is known concerning the relationship between initial tension and the character stress and strain fields, which determine the performance of piezoresistive-based transducers (*i.e.,* strain-gauge pressure sensors). Therefore, it is desirable to examine carefully the effects of internal stress on the structural behavior and linearity of these devices.

Several authors, including Nádai (1925) and Way(1934), examined the large deflection behavior for the pure plate case [discussed by Timoshenko and Woinowsky-Krieger(1959)]. Zheng and Zhou (1990) extended the work of Way by providing the general analytical formulas for axisymmetric plates subjected to compliant boundary conditions. Way (1934) and, also, McPherson *et al.* (1942) have conducted some experimental measurements on large metal plates. More recently, Voorthuyzen and Bergveld (1984) used a finite-difference model to investigate the large-deflection characteristics of circular plates subjected to in-plane loading over a limited dimensional domain. Allen (1986) investigated the effects of in-plane loads on the center deflection characteristics by employing energy methods. None of these studies, however, investigated the combined effects of non-linear loading and in-plane tension on the stress and strain fields. The present investigation deals specifically with the non-linear deflection field of a clamped, circular plate with an initial in-plane tension load[1], subjected to a uniform pressure load over its surface. In particular, the effects of varying the initial tensile load from zero (pure plate case) to very large values (pure membrane case) is explored. In the following section, the governing equations are developed and the appropriate non-dimensional scaling parameters identified. The small deflection characteristics and the transitions from pure plate to pure membrane behavior are detailed in §3. Section 4 contains the large deflection behavior and equivalent effects of initial tension and large loading, and the conclusions are presented in §5.

2 Basic Equations

Figure 1 shows a circular plate of radius a and thickness h, under an initial in-plane tension load, $N_r = N_0$ and a uniform transverse load $p_z = p_0$. The equilibrium equations for the symmetrical bending of this plate are

$$\frac{dN_r}{dr} + \frac{N_r - N_\theta}{r} = 0, \tag{1}$$

$$\frac{d}{dr}\left(rQ_r\right) + \frac{d}{dr}\left(rN_r\frac{dw}{dr}\right) + rp_0 = 0, \tag{2}$$

and

$$Q_r = \frac{dM_r}{dr} + \frac{M_r - M_\theta}{r}, \tag{3}$$

where N_r, N_θ are the lateral loads , Q_r is the shear force, M_r, M_θ are the bending moments per unit length, and w is the deflection of the plate in the z-direction. The radial and tangential mid-plane

[1] For an introduction to the alternate problem of in-plane compression, the "buckling problem", see Timoshenko and Woinowsky-Krieger (1959).

strains assuming von Kármán plate theory for large plate deflections are

$$\epsilon_r = \tfrac{du}{dr} + \tfrac{1}{2}\left(\tfrac{dw}{dr}\right)^2 \quad \text{and} \quad \epsilon_\theta = \tfrac{u}{r}, \tag{4}$$

where u is the radial displacement, while the radial and tangential curvatures are

$$\mathcal{K}_r = -\tfrac{d^2w}{dr^2} \quad \text{and} \quad \mathcal{K}_\theta = -\tfrac{1}{r}\tfrac{dw}{dr}. \tag{5}$$

The lateral loads and moments per unit length for large plate deflections are

$$N_r = A(\epsilon_r + \nu\epsilon_\theta), \qquad N_\theta = A(\epsilon_\theta + \nu\epsilon_r), \tag{6}$$

and

$$M_r = D(\mathcal{K}_r + \nu\mathcal{K}_\theta), \qquad M_\theta = D(\mathcal{K}_\theta + \nu\mathcal{K}_r), \tag{7}$$

where $A = Eh/(1-\nu^2)$ and $D = Eh^3/12(1-\nu^2)$ are the plate extensional and bending stiffnesses respectively, ν is Poisson's ratio, and E is the modulus of elasticity. Shearing deformations are neglected for the thin plates considered here ($h/a < 1/25$, Timoshenko and Woinowsky-Krieger (1959)).

These equations are reduced by first integrating (2),

$$Q_r + N_r\frac{dw}{dr} + \frac{p_0 r}{2} = 0, \tag{8}$$

and rewriting (4) in compatibility form,

$$r\frac{d\epsilon_\theta}{dr} + \epsilon_\theta - \epsilon_r + \frac{1}{2}\left(\frac{dw}{dr}\right)^2 = 0. \tag{9}$$

Substituting (5) into (7) and then into the moment equilibrium relation (3) gives

$$M_r = -D\left(\frac{d^2w}{dr^2} + \frac{\nu}{r}\frac{dw}{dr}\right), \tag{10}$$

$$M_\theta = -D\left(\frac{1}{r}\frac{dw}{dr} + \nu\frac{d^2w}{dr^2}\right), \tag{11}$$

and

$$Q_r = -D\left(\frac{d^3w}{dr^3} + \frac{1}{r}\frac{d^2w}{dr^2} - \frac{1}{r^2}\frac{dw}{dr}\right). \tag{12}$$

Placing (10 - 12) into (8) produces

$$\frac{d^3w}{dr^3} + \frac{1}{r}\frac{d^2w}{dr^2} - \frac{1}{r^2}\frac{dw}{dr} - \frac{N_r}{D}\frac{dw}{dr} = \frac{p_0 r}{2D}. \tag{13}$$

The inversion of (6) yields,

$$\epsilon_r = \tfrac{1}{Eh}(N_r - \nu N_\theta) \quad \text{and} \quad \epsilon_\theta = \tfrac{1}{Eh}(N_\theta - \nu N_r). \tag{14}$$

Substituting (14) into the compatibility relation (9) yields

$$\frac{dN_\theta}{dr} + \frac{dN_r}{dr} + \frac{Eh}{2r}\left(\frac{dw}{dr}\right)^2 = 0. \tag{15}$$

Further manipulation of (15) by introducing (1) produces,

$$\frac{dN_\theta}{dr} - \frac{N_r - N_\theta}{r} + \frac{Eh}{2r}\left(\frac{dw}{dr}\right)^2 = 0. \tag{16}$$

Equations (1), (13), and (16) represent three nonlinear equations in the three unknowns dw/dr, N_r, and N_θ. The nonlinearity appears in the $N_r dw/dr$ term in (13) and the $(dw/dr)^2$ term in (16).

For the problem in Fig. 1, the circular plate is first stretched by an in-plane tension load $N_r = N_\theta$ around its circumference and then subjected to a uniform load, p_0. The solution of the initial in-plane tension problem is obtained from the general equations (1 - 7) by setting $w = 0$ and $p_0 = 0$. This yields the following results,

$$N_r = N_\theta = N_0 \quad \text{and} \quad u = \tfrac{N_0}{Eh}(1-\nu)r, \tag{17}$$

which also satisfy the boundary condition, $N_r = N_0$ at $r = a$. Since $N_r = \sigma_r h$, where σ_r is the radial stress, the quantity $N_0/Eh = \sigma_r/E = \epsilon_0$ can be interpreted as the uniaxial strain in the material.

After being initially stretched by the load N_0, the plate is then subjected to the vertical load, p_0. For this case, the lateral loads are decomposed as follows:

$$N_r = N_0 + \tilde{N}_r \quad \text{and} \quad N_\theta = N_0 + \tilde{N}_\theta, \tag{18}$$

where $\tilde{N}_r$ and $\tilde{N}_\theta$ are incremental changes from N_0 and are functions of r. The placement of these expressions into (13), (1), (16) yields,

$$\frac{d^3w}{dr^3} + \frac{1}{r}\frac{d^2w}{dr^2} - \frac{1}{r^2}\frac{dw}{dr} - \frac{N_0}{D}\frac{dw}{dr} - \frac{\tilde{N}_r}{D}\frac{dw}{dr} = \frac{p_0 r}{2D}, \tag{19}$$

$$\frac{d\tilde{N}_r}{dr} + \frac{\tilde{N}_r - \tilde{N}_\theta}{r} = 0, \tag{20}$$

and

$$\frac{d\tilde{N}_\theta}{dr} - \frac{\tilde{N}_r - \tilde{N}_\theta}{r} + \frac{Eh}{2r}\left(\frac{dw}{dr}\right)^2 = 0. \tag{21}$$

It is convenient to non-dimensionalize these equations as follows:

$$\begin{aligned} &\xi = \tfrac{r}{a}, \qquad (\,)' = \tfrac{d}{d\xi}, \qquad W = \tfrac{w}{h}, \qquad U = \tfrac{u}{h} \\ &\theta = \tfrac{dW}{d\xi} = \tfrac{a}{h}\tfrac{dw}{dr}, \quad \Psi = \tfrac{d\theta}{d\xi} = \tfrac{a^2}{h}\tfrac{d^2w}{dr^2}, \quad S_r = \tfrac{\tilde{N}_r a^2}{Eh^3}, \quad S_\theta = \tfrac{\tilde{N}_\theta a^2}{Eh^3}. \end{aligned} \tag{22}$$

The non-dimensional forms of (19 - 21) are

$$\theta'' + \frac{\theta'}{\xi} - \left(k^2 + \frac{1}{\xi^2}\right)\theta - 12(1-\nu^2)S_r\theta = 6(1-\nu^2)P\xi, \tag{23}$$

$$S_r' + \frac{S_r - S_\theta}{\xi} = 0, \tag{24}$$

and

$$S_\theta' - \frac{S_r - S_\theta}{\xi} = -\frac{1}{2\xi}\theta^2, \tag{25}$$

where a non-dimensional tension parameter k, and a loading parameter P, have been introduced as,

$$k = \sqrt{\tfrac{N_0 a^2}{D}} = \tfrac{a}{h}\sqrt{\tfrac{12(1-\nu^2)N_0}{Eh}} \quad \text{and} \quad P = \tfrac{p_0 a^4}{Eh^4}. \tag{26}$$

The corresponding non-dimensional in-plane displacement U as obtained from (4) and (14) and the vertical displacement W as obtained by integration, are then,

$$U = \frac{u}{h} = \frac{h}{a}(S_\theta - \nu S_r)\xi \tag{27}$$

and

$$W = \frac{w}{h} = \int \theta d\xi. \tag{28}$$

Equations (23) - (25) are subject to following boundary conditions:

$$@\ \xi = 0: \qquad \theta = 0, \qquad S_r = S_\theta. \tag{29}$$

and

$$@\ \xi = 1: \qquad \theta = 0, \qquad U = \tfrac{h}{a}(S_\theta - \nu S_r) = 0. \tag{30}$$

which represent symmetry conditions at the center and clamped conditions at the edge of the plate.

The corresponding radial stress field in the plate is found from the definitions of the stress resultants,

$$\sigma_r = \frac{N_r}{h} + \frac{12 M_r z}{h^3}, \tag{31}$$

where the extrema occur at the top and bottom surfaces, $z = \pm h/2$. The non-dimensional form is obtained by making use of (10) and (18),

$$\sigma_r = \frac{N_0}{h} + \frac{Eh^2}{a^2}\left[S_r - \frac{z}{h(1-\nu^2)}\left(\Psi + \frac{\nu\theta}{\xi}\right)\right]. \tag{32}$$

The first term represents the initial stress, the second the membrane stress, and the third the bending stress. The corresponding strains ϵ_r in the plate is obtained from (14) and (18),

$$\epsilon_r = \frac{1}{Eh}(N_r + \nu N_\theta) + z\mathcal{K}_r. \tag{33}$$

The non-dimensional form is obtained by making use of (5),

$$\epsilon_r = (1-\nu)\frac{N_0}{Eh} + \left(\frac{h}{a}\right)^2\left[S_r - \nu S_\theta - \frac{z}{h}\Psi\right]. \tag{34}$$

The corresponding tangential stress (σ_θ) and strain (ϵ_θ) fields can be obtained through similar manipulations.

3 Linear Theory

Before investigating the nonlinear behavior (23 - 25), it is informative to look at the small deflection, linear behavior of these equations as the tension parameter k varies from 0 to ∞. For small deflections, the mid-plane load S_r is assumed small, so that the nonlinear $S_r\theta$ term in (23) can be neglected. Multiplying (23) by ξ^2 then leads to the linear equation[2],

$$\xi^2\theta'' + \xi\theta' \ - (1 + k^2\xi^2)\theta = 5.56 P\xi^3, \tag{35}$$

which is a modified Bessel equation possessing the general solution,

$$\theta(\xi) = C_1 I_1(k\xi) + C_2 K_1(k\xi) - \frac{5.56 P\xi}{k^2}, \tag{36}$$

where $I_1(k\xi)$ and $K_1(k\xi)$ are modified Bessel functions of the first kind and second kind, respectively (Abramowitz and Stegun, 1972). The requirement of a bounded solution at $\xi = 0$ and implementation the boundary conditions (29 - 30) yields,

$$\theta(\xi) = 5.56 P\left[\frac{I_1(k\xi)}{k^2 I_1(k)} - \frac{\xi}{k^2}\right]. \tag{37}$$

[2] In this and all subsequent equations, the Poisson ratio is taken as $\nu = 0.27$, which is typical of silicon nitride. Small modifications can be made for other values of ν.

The corresponding deflection is obtained by integrating (37),

$$W(\xi) = 2.78P\left[\frac{2\big(I_0(k\xi) - I_0(k)\big)}{k^3 I_1(k)} + \frac{1-\xi^2}{k^2}\right]. \tag{38}$$

Two limiting cases are of interest here. For the case of a pure plate ($k = 0$), (35) becomes an equidimensional ordinary differential equation possessing the following solutions:

$$\theta(\xi) = -0.695P\xi(1-\xi^2) \tag{39}$$

and

$$W(\xi) = 0.174P(1-\xi^2)^2. \tag{40}$$

For the other case of a pure membrane, $k \to \infty$, only the $k^2\xi^2\theta$ term remains on the left hand side of Equation 35. The resulting equation is integrated to yield,

$$\theta(\xi) = -\frac{5.56P\xi}{k^2} \tag{41}$$

and

$$W(\xi) = \frac{2.78P}{k^2}(1-\xi^2). \tag{42}$$

Equations (39 - 42) can also be obtained by taking the small and large argument limit of the modified Bessel solutions (37 - 38).

The effect of initial in-plane tension is shown by plotting the center deflection, W_0, as a function of tension parameter (see Fig. 2). In this figure, (40) and (42) form two asymptotes to the deflections obtained from (38). There appears to be a transition from plate behavior to membrane behavior in the region from $k \approx 1$ to $k \approx 20$. The corresponding change in deflection shape is shown in Fig. 3. As the tension parameter increases, one notes the sharp change in curvature near the edge, $\xi \approx 1$, in order to accommodate the zero slope boundary condition there.

A better understanding of the transition to membrane behavior is gained by introducing the large value approximation for the modified Bessel functions, namely (Abramowitz and Stegun, 1972),

$$\lim_{z\to\infty} I_\nu(z) \approx \frac{e^z}{\sqrt{2\pi z}}, \quad \forall \ \ \nu. \tag{43}$$

The placement of this approximation into (37) and (38) produces for large k,

$$\theta(\xi) \approx \frac{-5.56P}{k^2}\left[\xi - \frac{e^{-k(1-\xi)}}{\sqrt{\xi}}\right] \tag{44}$$

and

$$W(\xi) \approx \frac{2.78P}{k^2}\left[1-\xi^2 - \frac{2}{k}\left(1 - \frac{e^{-k(1-\xi)}}{\sqrt{\xi}}\right)\right]. \tag{45}$$

These equations indicate small exponential edge-zone corrections to the pure membrane case (41) and (42), to accommodate the zero slope condition at $\xi = 1$. Figure 4 shows the slope θ plotted versus non-dimensional radius ξ for increasing values of k. The extent of this edge zone[3], $\Delta\xi$, gets smaller as k increases and is estimated by assuming that the exponential decays to 5% of its maximum value,

$$\Delta\xi \approx \frac{3}{k}. \tag{46}$$

Furthermore, the change in center deflection, W_0, from the pure membrane case is approximated from (45) as

$$W_0 \approx \left[1 - \frac{2}{k}\right](W_0)_{mem}. \tag{47}$$

[3] Friedrichs (1949) first noted the development of an edge zone region with rapidly changing properties in his study of plate deflections.

The corresponding stresses σ_r and strains ϵ_r in the plate are found from (32) and (34). For linear theory, the main contributions to the stress and strain fields come from the initial stress and the bending forces, the later of which are dominated by the curvature term Ψ, namely,

$$\Psi = 5.56P\left[\frac{I_0(k\xi)}{kI_1(k)} - \frac{1}{k^2\xi}\frac{I_1(k\xi)}{I_1(k)} - \frac{1}{k^2}\right]. \tag{48}$$

The large k approximation of (48) is

$$\Psi \approx \frac{5.56P}{k^2}\left[-1 + \frac{k\xi - 1}{\xi^{3/2}}e^{-k(1-\xi)}\right], \tag{49}$$

which represents the membrane solution plus a small exponential edge zone correction. Figure 5 shows the curvature term plotted versus radius for different values of the tension parameter. For large k, the maximum curvature term at the edge is,

$$\Psi \approx \frac{5.56P}{k} \tag{50}$$

which is considerably greater than the membrane curvature, $\Psi = -5.56P/k^2$ occurring at the center and over most of the remaining portion of the plate. Physically, this indicates the presence of a stress concentration near the clamped plate boundary (for example, (32)).

4 Nonlinear Theory

For large deflections ($W >> 1$), nonlinear behavior arises when the incremental mid-plane forces, $\tilde{N}_r$, $\tilde{N}_\theta$, are no longer negligible. This behavior is manifested by the θ^2 term in (25) changing the mid-plane force S_r, which in turn affects the deflection equations through the nonlinear $S_r\theta$ term in (23).

A convenient way of numerically solving this nonlinear system is to combine (24 - 25) and recast (23 - 25) as two coupled, second-order equations in the variables θ and S_r (Voorthuyzen and Bergveld, 1984),

$$\xi^2\theta'' + \xi\theta' - \left[1 + \xi^2(k^2 + 11.12S_r)\right]\theta = 5.56P\xi^3, \tag{51}$$

$$\xi^2 S_r'' + 3\xi S_r' = -\frac{\theta^2}{2}. \tag{52}$$

The corresponding boundary conditions from (29) and (30) now become

$$@\ \xi = 0: \qquad \theta = 0, \qquad S_r' = 0, \tag{53}$$

$$@\ \xi = 1: \qquad \theta = 0, \qquad S_r' + 0.73S_r = 0. \tag{54}$$

Prior to discretizing (51-54), the following coordinate transform pair was used to refine the mesh in the edge zone region (46),

$$\xi = 1 - \frac{(\beta+1) - (\beta-1)\left[\frac{\beta+1}{\beta-1}\right]^{\overline{\xi}}}{\left[\frac{\beta+1}{\beta-1}\right]^{\overline{\xi}} + 1} \qquad \text{and} \qquad \overline{\xi} = -\frac{\ln\frac{\beta-\xi}{\beta+\xi}}{\ln\frac{\beta+1}{\beta-1}}, \tag{55}$$

where ξ is the physical plane with grid points clustered near $\xi = 1$, $\overline{\xi}$ is the uniformly spaced computational plane, and β is the stretching parameter (Roberts, 1971). This stretching transform clusters more points near $\xi = 1$ as β approaches 1. In the present study, a value of $\beta = 1.05$ was

used to capture the physics of the edge-zone by clustering 30% of the grid points in the region $0.9 < \xi < 1.0$. The transformed versions of (51 - 54) are

$$\xi(\overline{\xi})^2\left(\frac{d\overline{\xi}}{d\xi}\right)^2\frac{d^2\theta}{d\overline{\xi}^2}+\left[\xi(\overline{\xi})\frac{d\overline{\xi}}{d\xi}+\xi(\overline{\xi})^2\left(\frac{d^2\overline{\xi}}{d\xi^2}\right)\right]\frac{d\theta}{d\overline{\xi}}-\left[1+\xi(\overline{\xi})^2(k^2+11.12S_r(\overline{\xi}))\right]\theta(\overline{\xi})=5.56P\xi(\overline{\xi})^3, \quad (56)$$

$$\xi(\overline{\xi})^2\left(\frac{d\overline{\xi}}{d\xi}\right)^2\frac{d^2S_r}{d\overline{\xi}^2}+\left[3\xi(\overline{\xi})\frac{d\overline{\xi}}{d\xi}+\frac{d^2\overline{\xi}}{d\xi^2}\right]\frac{dS_r}{d\overline{\xi}}=-\frac{\theta(\overline{\xi})^2}{2}, \quad (57)$$

and

$$@\ \overline{\xi}=0: \qquad \theta=0, \qquad \tfrac{d\overline{\xi}}{d\xi}\tfrac{dS_r}{d\overline{\xi}}=0, \quad (58)$$

$$@\ \overline{\xi}=1: \qquad \theta=0, \qquad \tfrac{d\overline{\xi}}{d\xi}\tfrac{dS_r}{d\overline{\xi}}+0.73S_r=0. \quad (59)$$

Equations (56) and (57) were then discretized using 2^{nd}-order accurate central-difference schemes, while the derivative and mixed boundary conditions were implemented by using 2^{nd}-order accurate forward- and backward-differencing schemes, respectively (for example, Anderson *et al.*, 1984). The computational domain consisted of a radial mesh containing 101 points to provide adequate resolution in the edge zone. In matrix form, (56) and (57) are represented as

$$\left[\mathcal{A}(S_r)\right]\Theta=\mathcal{C}, \quad (60)$$

$$\left[\mathcal{B}\right]\mathcal{S}_r=\frac{1}{2}\Theta^2, \quad (61)$$

where $\left[\mathcal{A}(S_r)\right]$ and $\left[\mathcal{B}\right]$ are square matrices in tridiagonal form. This nonlinear system was then solved using an implicit iteration technique similar to that used by Voorthuyzen & Bergveld (1984). For a given k, (61) can be readily solved by direct inversion provided Θ is known, since $[\mathcal{B}]$ is in modified tridiagonal form. In the present study, the linear solution was used as an initial guess (see (37)). Once determined, $\mathcal{S}_r$ was then substituted into (60) and was again inverted to produce an updated Θ. The updated Θ was first corrected by employing an under-relaxation technique (see, for example, Anderson *et al.*, 1984) and then substituted into (61) producing a new $\mathcal{S}_r$. In this study, an under-relaxation parameter of 0.2 was used to accelerate convergence. This iterative process was repeated until the the solution converged to within a tolerance of 0.5%. Finally, the variables W, Ψ, S_θ, and U were then determined by employing 2^{nd}-order accurate differencing schemes for the differentiation and integration operators.

Results of the nonlinear calculations for the deflection, deflection curvature, and in-plane load at the center of the plate are given in Figs. 6 to 9. Figure 6 shows the variation of the center deflection with loading. For the zero initial tension case, $k = 0$, the deflection scaling changes from the linear $W_0 \sim P$ at low loading levels to $W_0 \sim P^{1/3}$ at high loading. The numerical results for center-deflection characteristics agree very well with those given by Nádai (1925) for $k = 0$ and with Voorthuyzen & Bergveld (1984) and Allen (1986) for $k > 0$. For the cases with $k > 0$, the curves start from their respective linear values and become asymptotic to the $k = 0$ case. In addition, the onset of nonlinearity is delayed with increasing k. This effect is better illustrated by plotting the maximum loading, P_{max}, that will produce a 5% departure from linearity in the center deflection, as a function of k (see Fig. 7). The delay of the onset of nonlinear behavior with increasing k scales according to $P_{max} \sim k^3$. Figure 8 shows the variation of the curvature at the plate center, Ψ_0, with loading. Again, for the $k = 0$ case, the curvature scaling changes from $\Psi_0 \sim P$ at low loads to $\Psi_0 \sim P^{1/3}$ at high loads, but there appears a small bump in the transition. The $k > 0$ cases again merge asymptotically into the $k = 0$ case. Figure 9 shows the variation of the in-plane load at the plate center with loading. For the $k = 0$ case, the in-plane load developed in the plate is always nonlinear and changes from $S_r \sim P^2$ at low loadings to $S_r \sim P^{2/3}$ at higher loadings. This behavior is attributed to the Θ^2 term present in (57) which determines S_r. The cases with initial tension also merge asymptotically into the $k = 0$ case.

The distribution of the deflection, slope, and curvature in the plate for the $k = 0$ case are given in Figs. 10 to 12. Figure 10 shows the deflection distributions in the plate at different values of loading. The $P = 1$ case represents the linear bending behavior (see Fig. 7), while for higher loadings, large in-plane loads develop and the deflections tend to exhibit membrane behavior shown earlier in Fig. 3. Similar trends with loading are apparent for the nonlinear slope and curvature distributions given in Figs. 11 and 12. These trends in Figs. 11 and 12 are similar to those found in Figs. 4 and 5. The corresponding distribution of in-plane loads and in-plane deflection for the $k = 0$ case are shown in Figs. 13 to 15. The in-plane loads plotted in Figs. 13 and 14 **become** more uniform at the higher loads, although never quite constant. Interestingly, Fig. 15 demonstrates that the in-plane deflection becomes negative near the edge of the plate.

The similar influences of large P and large k discussed above can be traced to the $(k^2+11.12S_r)$ term in (56). Therefore, an equivalent linear tension parameter, k_E, is defined as,

$$k_E = \sqrt{k^2 + 11.12S_r}, \tag{62}$$

where S_r is taken as $S_r \approx S_r(0)$ and k_E is now only a function of P and k (see Fig. 9). The equivalent tension parameter k_E is plotted as a function of loading **in** Fig. 16. For any given P and k combination, Fig. 16 determines the equivalent tension parameter, k_E, which in turn identifies the appropriate deflection, slope, and curvature distribution characteristics from the basic linear theory, (37, 38, and 48) or Figs. 3 - 5. Also, k_E can be used in the convenient approximations of (46), (47), and (50). Alternatively, by moving the given (P, k) point on Fig. 16 horizontally to the right to the $k = 0$ case, one obtains the loading P which identifies the appropriate distribution characteristics from the previous $k = 0$ nonlinear theory, Figs. 10 - 15. The basic values of W_0, Ψ_0, and $S_r(0)$ for a given (P, k) are obtained from Figs. 6, 8 and 9.

Figure 16 shows that the nonlinear P= 1, 10, 100, 1000, 10,000, 100,000 cases for $k = 0$ calculated here (Figs. 10 - 15) correspond approximately to the linear $k = 1, 5, 10, 20, 50, 100$ cases[4] (Figs. 3 - 5). They have similar distribution behavior, particularly with regards to the extent of the edge zone. The slight variation in Θ/W_0 arises from S_r varying slightly across the plate instead of remaining constant at S_0. Figure 16 also displays a dotted line which indicates the extent of the linear region, mentioned previously (see Fig. 7). For a given value of k, points to the right of the dotted line indicate a departure from linearity greater than 5% for the center deflections. All points to the left of the dotted line indicate linear theory is valid.

5 Conclusions

The large deflections of a clamped circular plate have been investigated over a wide range of transverse loadings and initial in-plane tension loads. The transition from plate behavior to membrane behavior for small deflections is a function of the initial tension parameter, k. This transition occurs over the range $1 < k < 20$, with plate behavior dominating for $k < 1$. For $k > 20$, membrane behavior dominates the majority of the clamped plate, however, a narrow edge-zone region develops near $\xi = 1$ to meet the zero-slope boundary condition. Simple estimates of this edge zone and its properties are given. In addition, the loading limits for the validity of small deflection, linear theory are presented as a function of the initial tension parameter. The similar effects of large initial in-plane tension k and large loadings P are combined into a single equivalent tension parameter, k_E, which conveniently characterizes the plate behavior. The equivalent tension parameter permits the use of the closed-form, linear solutions to characterize the nonlinear behavior of the plate.

The values and trends presented in this study are useful aids for the design of thin, circular disks often found in microelectromechanical systems. For example, the results in §3 imply that

[4] The $k = 1$ case is essentially identical to the $k = 0$ case (see Fig. 2).

the non-dimensional sensitivity of deflection-based pressure sensors ($W_0/P \sim 1/k^2$) and the sensitivity piezoresistive-based pressure sensors ($\Psi_{\xi=1}/P \sim 1/k$) scale differently with initial tension. In addition, for piezoresistive transducers the edge-zone scaling indicates the extent of the stress concentration region and thus dictates the placement and size of the piezoresistors. Finally, the scaling law regarding limits of linear theory with increasing initial tension indicate that the loss of sensitivity with increasing dimensional tension can be offset by a subsequent increase in thickness ratio.

6 Acknowledgments

This work has been sponsored by NASA-Langley Research Center under grant NAG-1-1785, (monitored by John M. Seiner). The authors would like to thank Lalitha Parameswaran, Kenneth S. Breuer, Stephen D. Senturia, and Martin A. Schmidt for their helpful comments.

7 References

Allen, M.G., "Measurement of Mechanical Properties and Adhesion of Thin Polyimide Films," M.S. Thesis, MIT, Cambridge, MA, 1986.

Abramowitz, M. and Stegun, I.A. *Handbook of Mathematical Functions*, 9^{th} ed., Dover, New York, 1972.

Anderson, D.A., Tannehill, J.C., and Pletcher, R.H., *Computational Fluid Mechanics and Heat Transfer*, Hemisphere, New York, 1984.

Chau, H-L. and Wise, K.D., "Scaling Limits in Batch-Fabricated Silicon Pressure Sensors," *IEEE Transaction of Electron Devices*, Vol. ED-34, 1987, pp. 850-858.

Cho, S.T., Najafi, K., and Wise, K.D., "Internal Stress Compensation and Scaling in Ultrasensitive Silicon Pressure Sensors," *IEEE Transaction of Electron Devices*, Vol. 39, No 4, 1992, pp. 836-842.

Clark, S.K. and Wise, K.D., "Pressure Sensitivity in Anisotropically Etched Thin-Diaphragm Pressure Sensors," *IEEE Transaction of Electron Devices*, Vol. ED-26, No 12, 1979, pp. 1887-1896.

Friedrichs, K.O., "The Edge Effect In Bending and Buckling with Large Deflections," *Proceedings of Symposia in Applied Mathematics*, Vol. 1, Non-Linear Problems in Mechanics of Continua, American Mathematical Society, New York, 1949, pp. 188-193.

Löfdahl, L., Kälvesten, E., and Stemme, G., "Small Silicon Based Pressure Transducers for Measurements in Turbulent Boundary Layers," *Experiments in Fluids*, Vol. 17, 1994, pp. 24-31.

McPherson, A., Ramberg, W., and Levy, S., "Normal-Pressure Tests of Circular Plates with Clamped Edge," *NACA Technical Report 744*, 1942.

Nádai, A., *Elastisclie Platten*, Julius Springer, Berlin, 1925, pp. 288.

Roberts, G.O., "Computational Meshes for Boundary Layer Problems," *Lecture Notes in Physics*, Vol. 8, Springer-Verlag, New York, 1971, pp. 171-177.

Schellin, R. and Hess, G., "A Silicon Subminiature Microphone Based on Piezoresistive Polysilicon Strain Gauges," *Sensors and Actuators A*, Vol. 32, 1992, pp. 555-559.

Sze, S.M., *Semiconductor Sensors*, John Wiley & Sons, New York, 1994.

Timoshenko, S.P. and Woinowsky-Krieger, S., *Theory of Plates and Shells*, 2^{nd} ed., McGraw-Hill, New York, 1959.

Voorthuyzen, J.A. and Bergveld, P., "The Influence of Tensile Forces on the Deflection of Circular Diaphragms in Pressure Sensors," *Sensors and Actuators A*, Vol. 6, 1984, pp. 201-213.

Way, S., "Bending of Circular Plates with Large Deflection," *Trans. ASME*, Vol. 56, 1934, pp. 627-636.

Zhen, X. and Zhou, Y., "Analytical Formulas of Solutions of Geometrically Nonlinear Equations of Axisymmetric Plates and Shallow Shells,", *Acta Mechanica Sinca*, Vol. 6, No. 1, 1990.

List of Figures

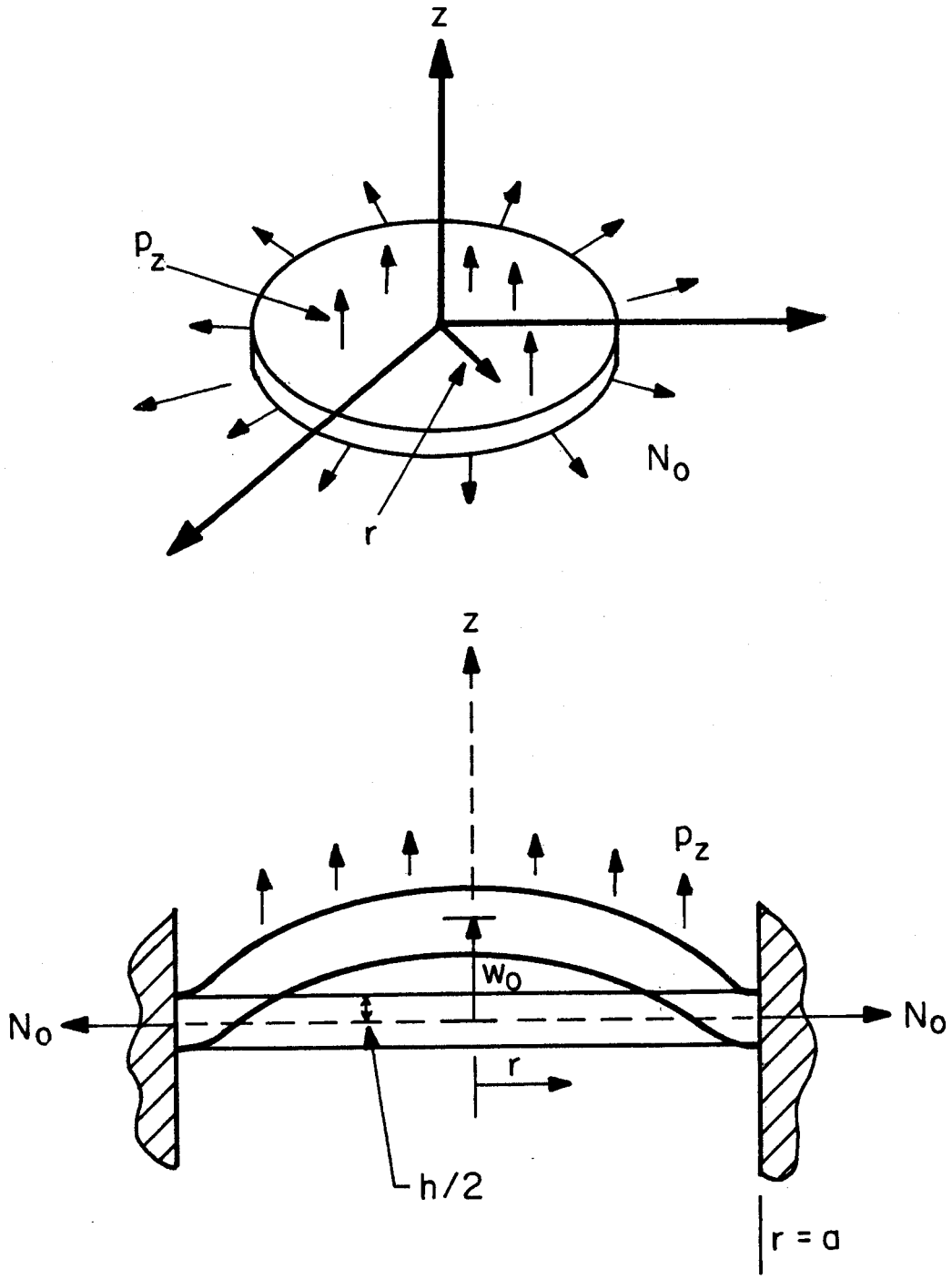

Figure 1: Schematic of clamped circular disk with initial in-plane tension.

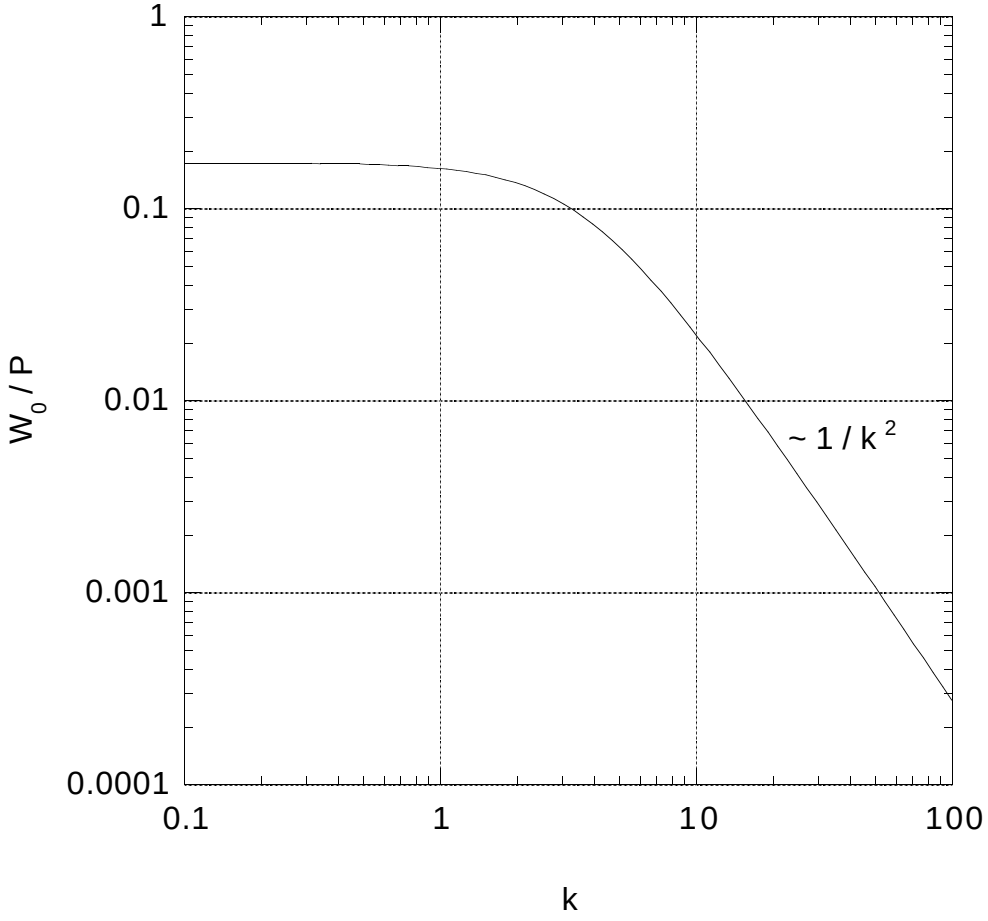

Figure 2: Center deflection normalized by loading as a function of in-plane tension.

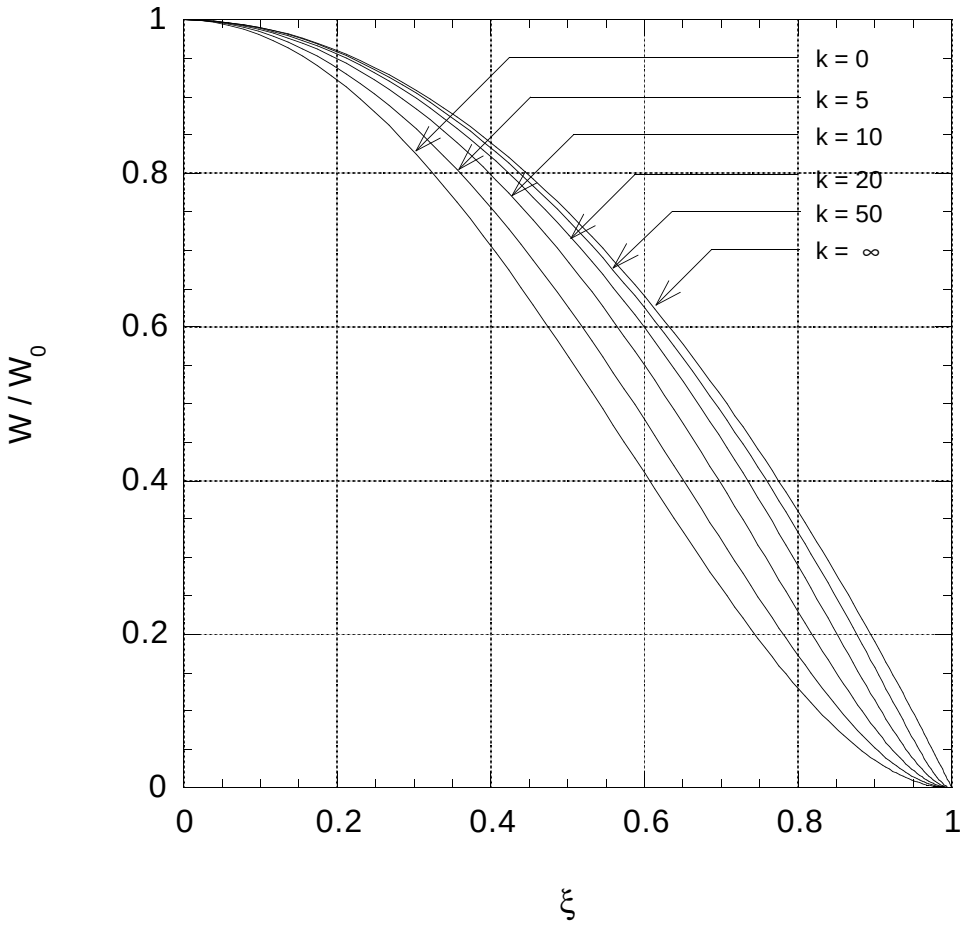

Figure 3: Normalized deflection as a function of radial distance for several values of k.

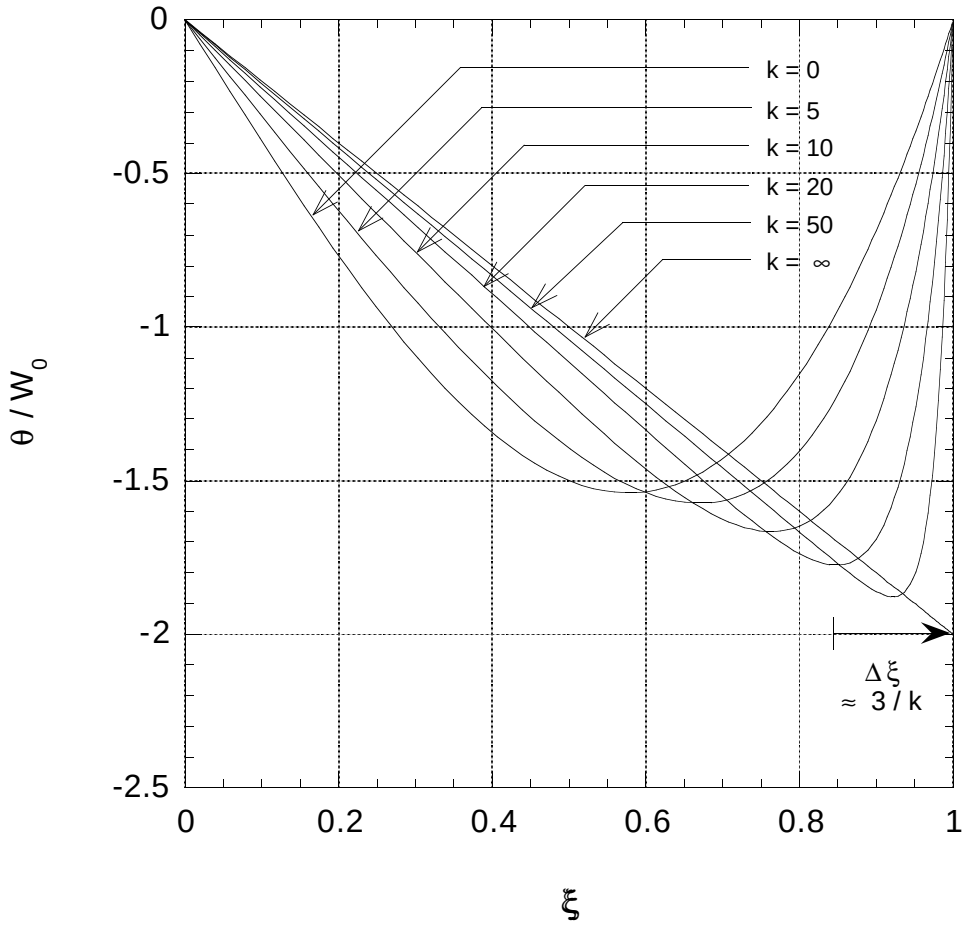

Figure 4: Normalized deflection slope as a function of radial distance for several values of k.

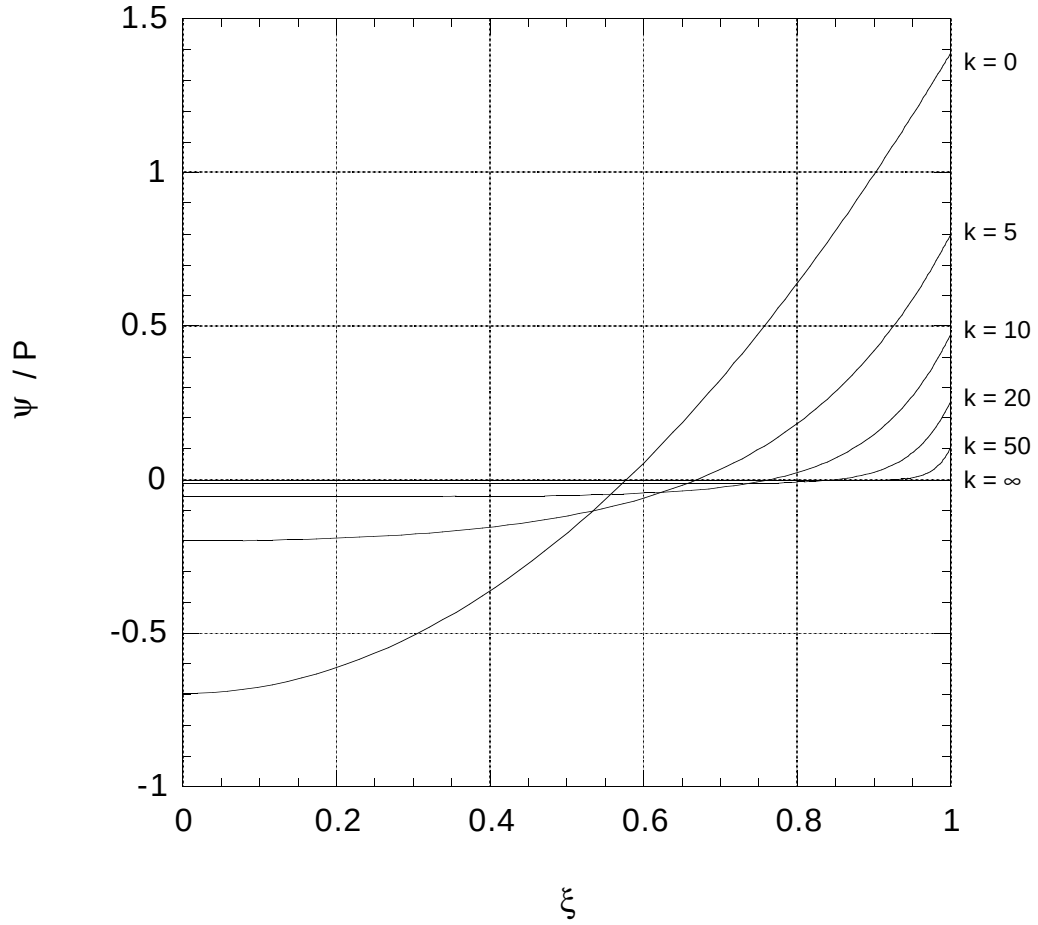

Figure 5: Normalized deflection curvature as a function of radial distance for several values of in-plane tension.

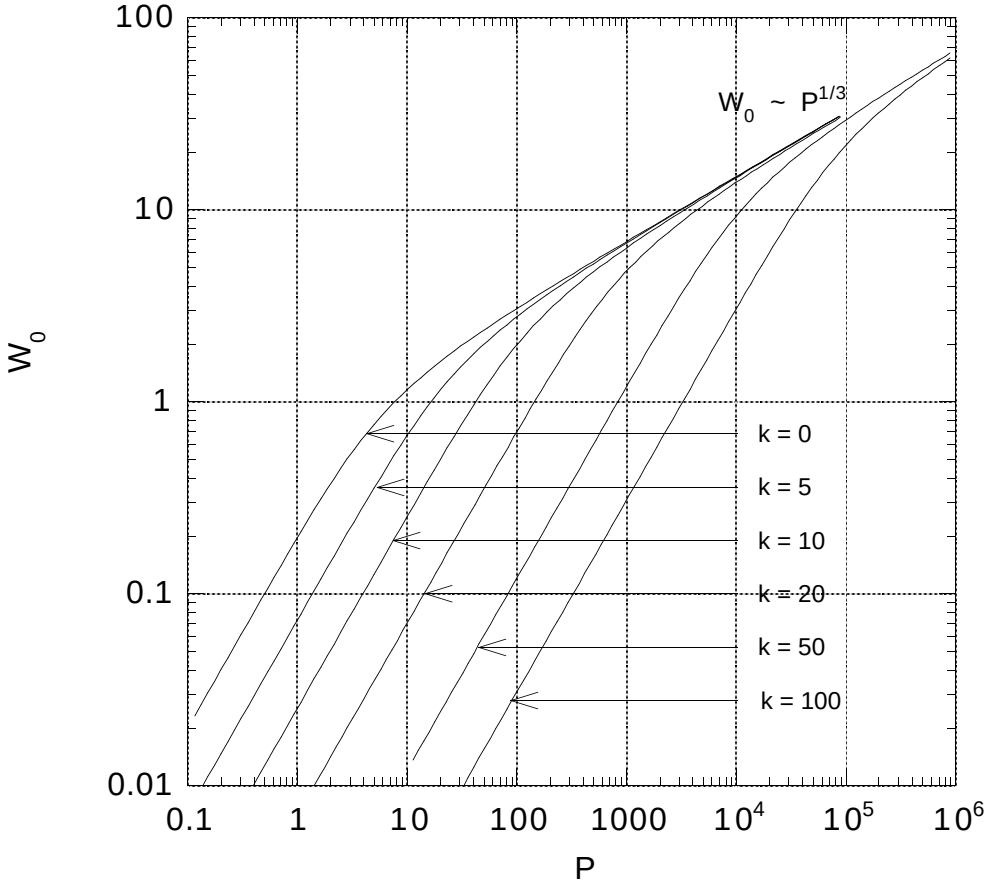

Figure 6: Center deflection as a function of loading for several values of in-plane tension.

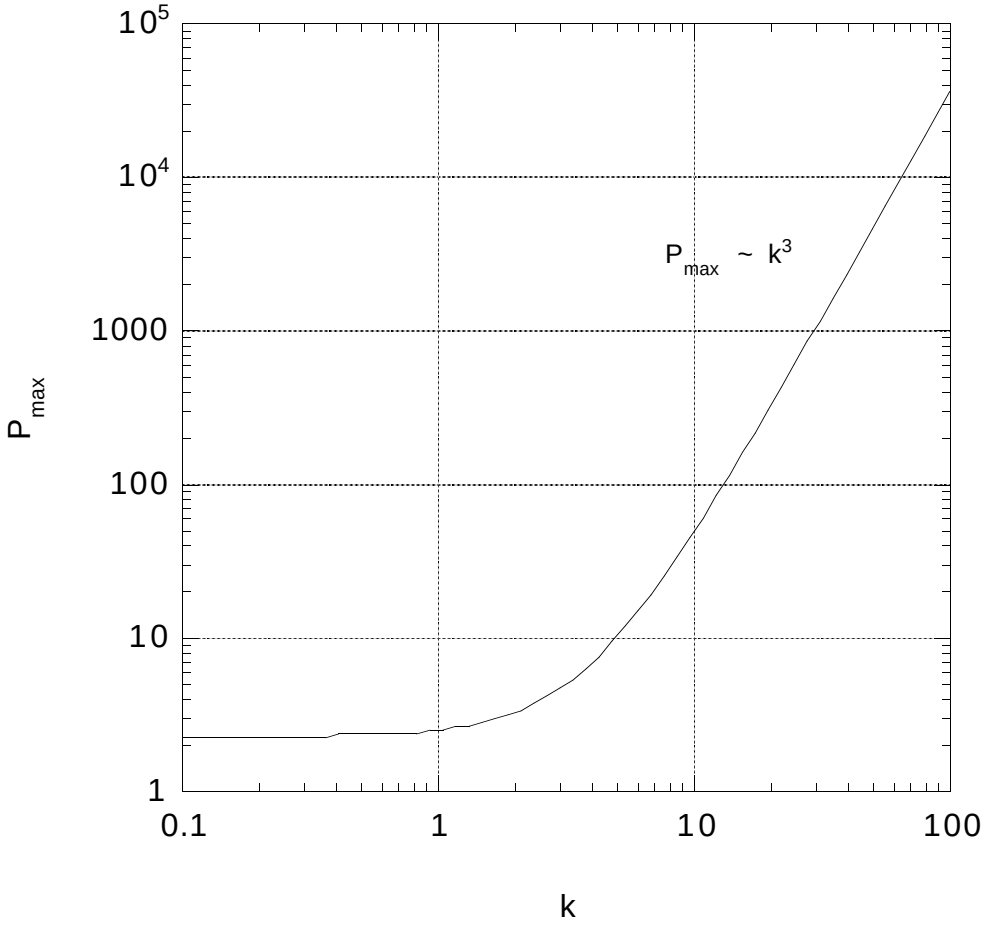

Figure 7: Maximum linear loading as a function of in-plane tension.

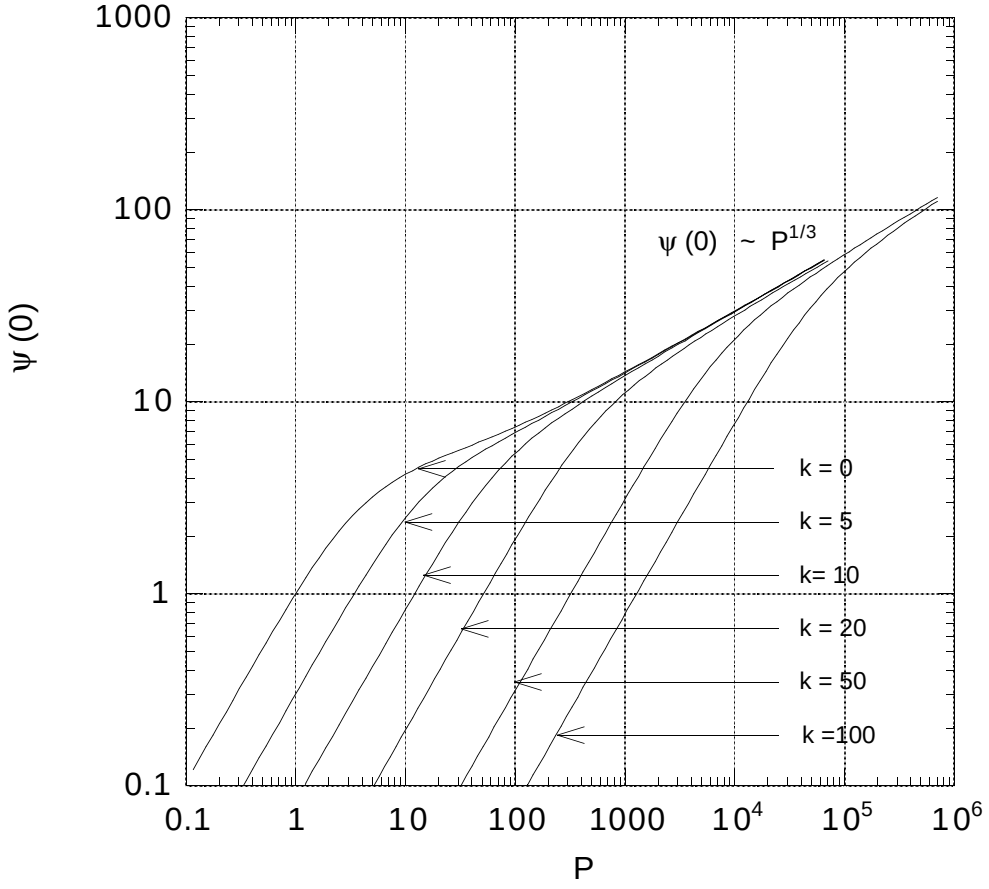

Figure 8: Center deflection curvature as a function of loading for several values of in-plane tension.

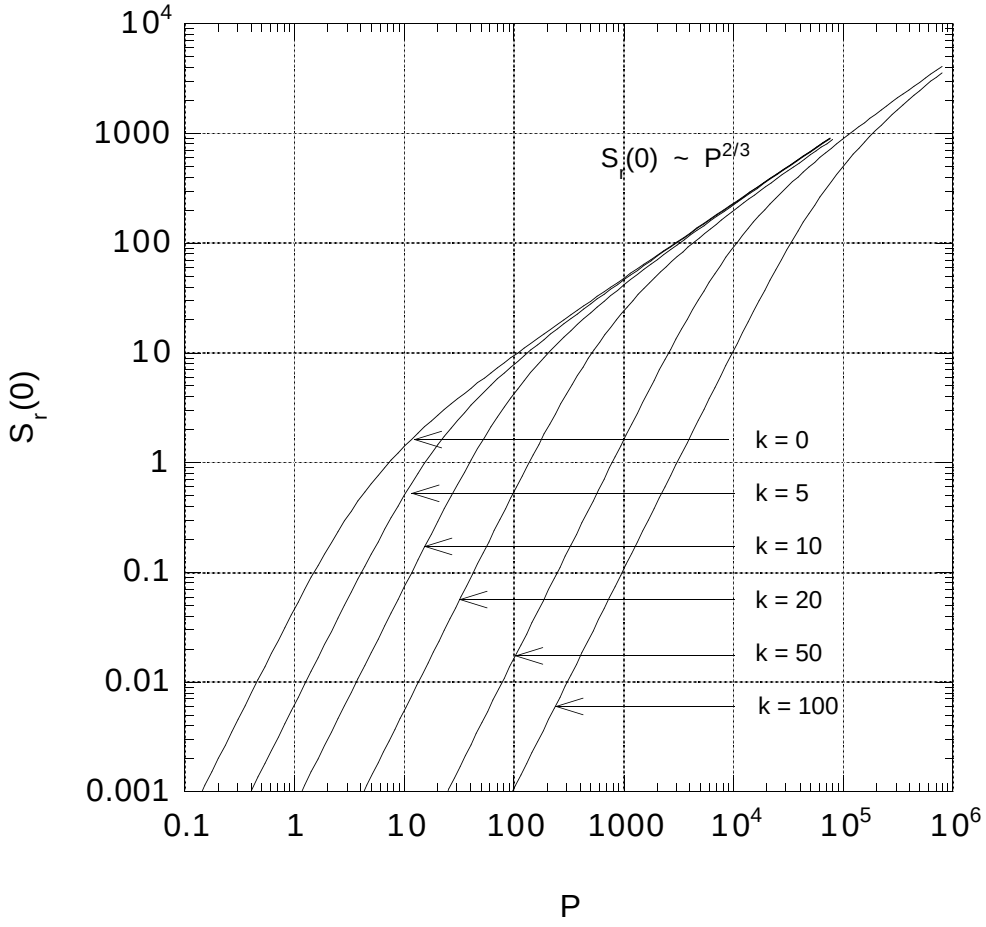

Figure 9: Center in-plane stress as a function of loading for several values of in-plane tension.

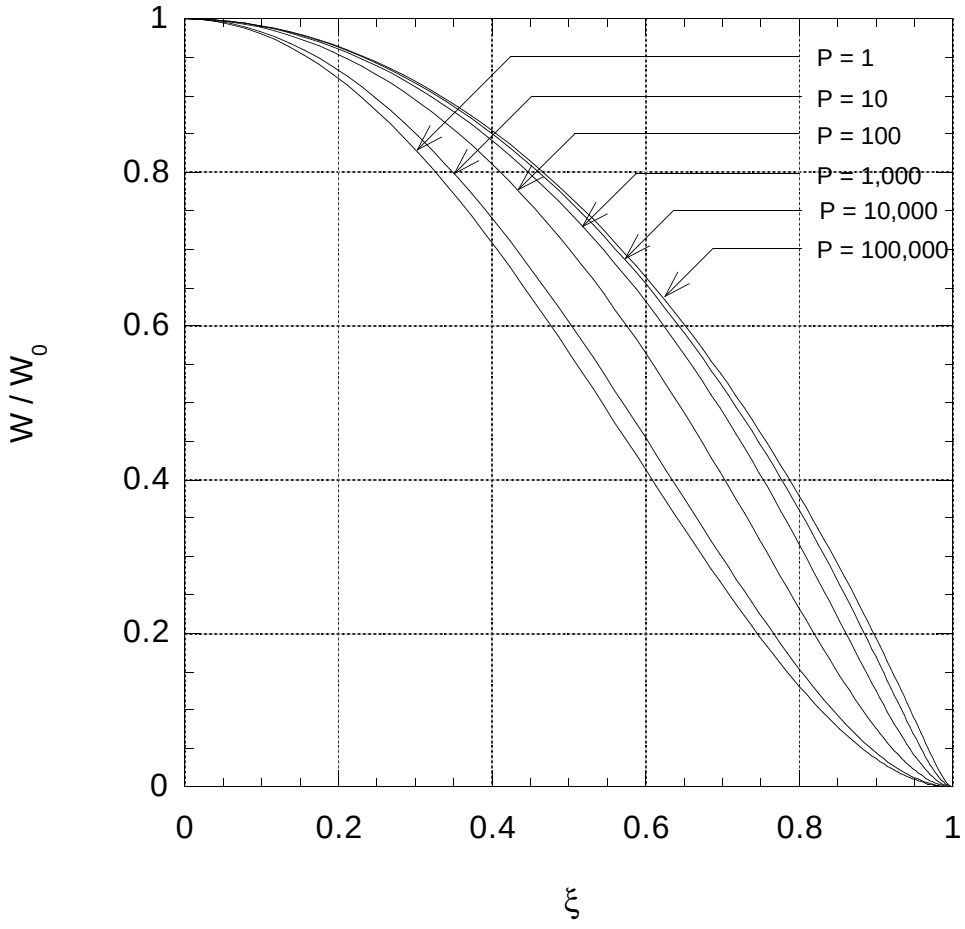

Figure 10: Normalized deflection as a function of radial distance for several values of loading ($k = 0$).

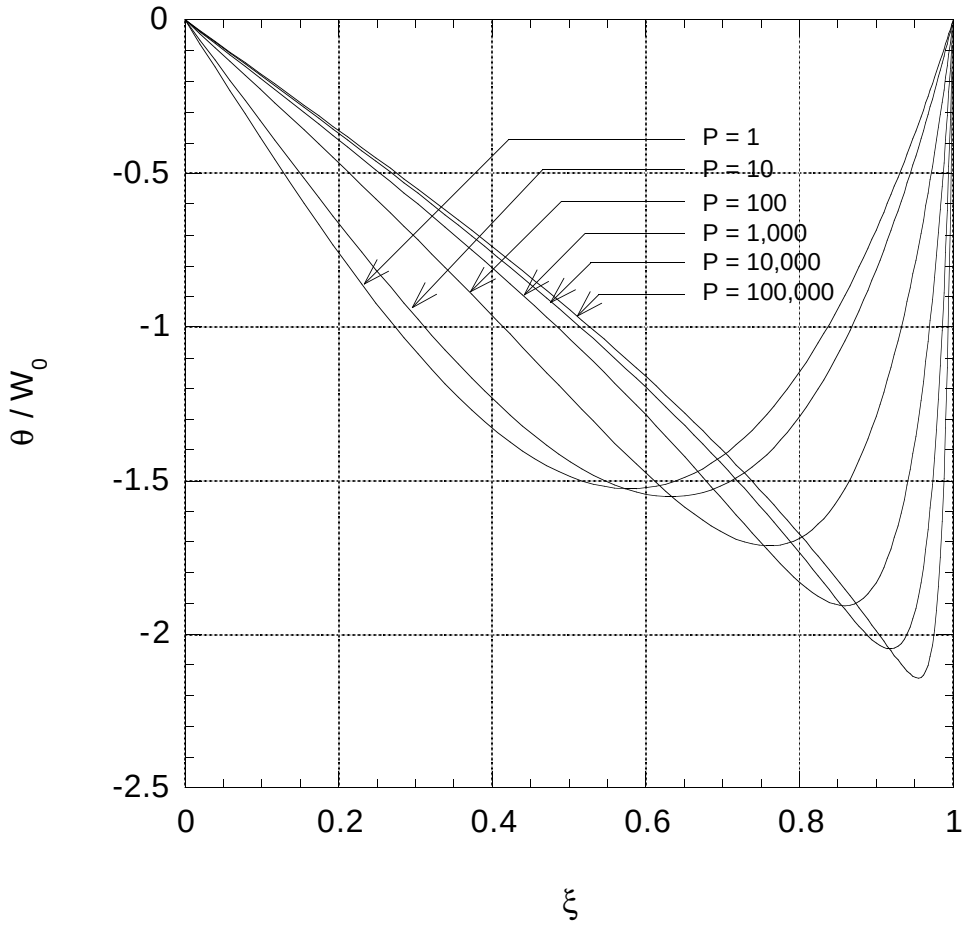

Figure 11: Normalized deflection slope as a function of radial distance for several values of loading ($k = 0$).

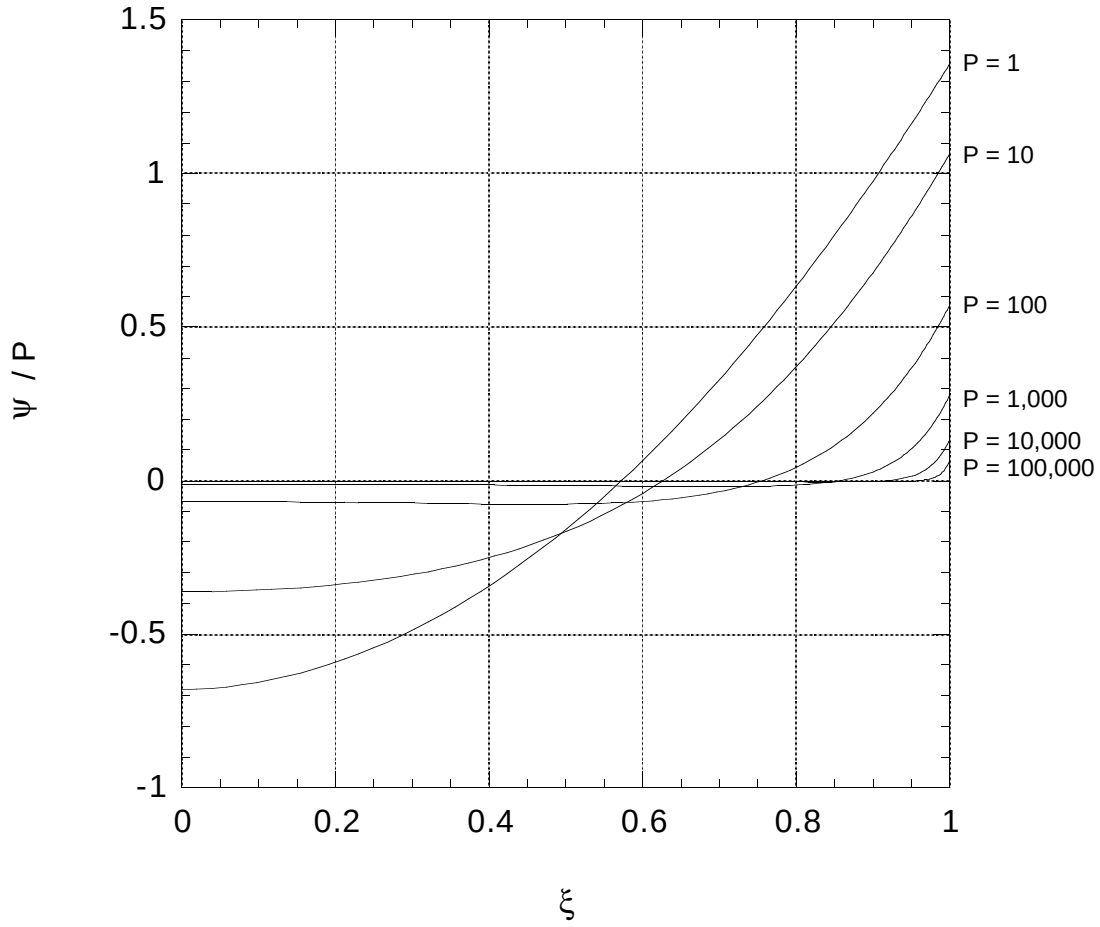

Figure 12: Normalized deflection curvature as a function of radial distance for several values of loading ($k = 0$).

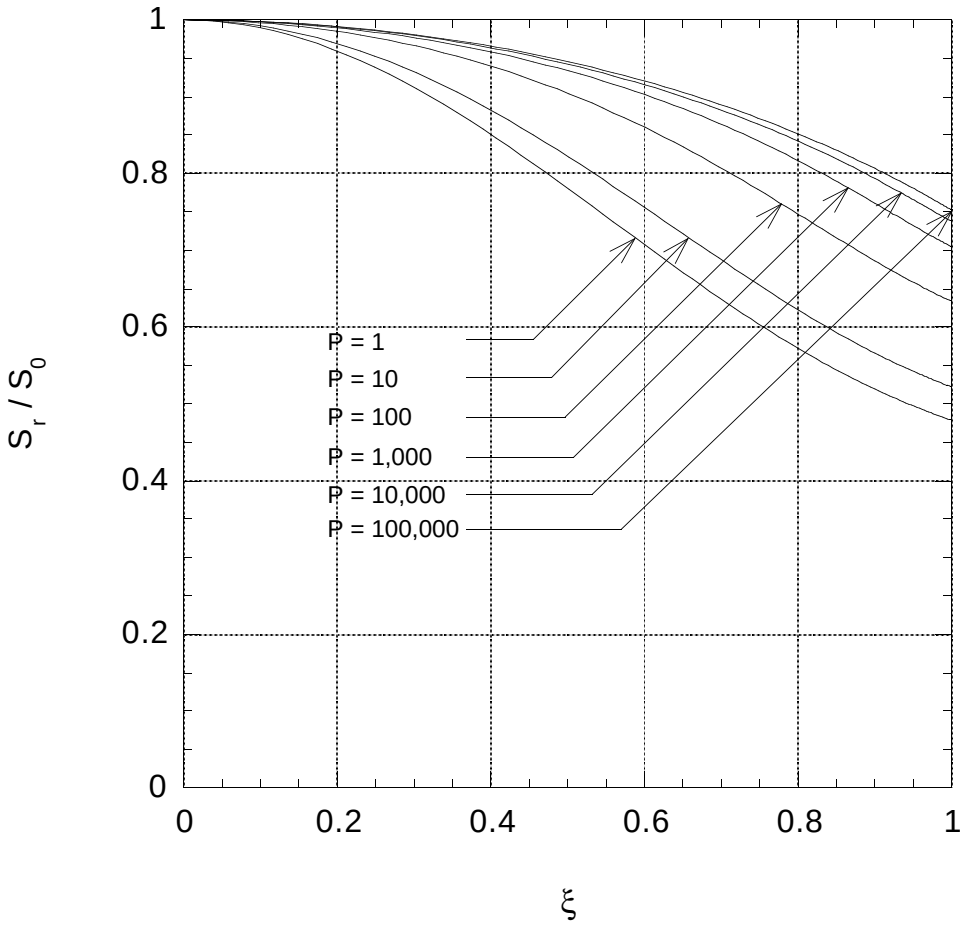

Figure 13: Normalized in-plane radial stress as a function of radial distance for several values of loading ($k = 0$).

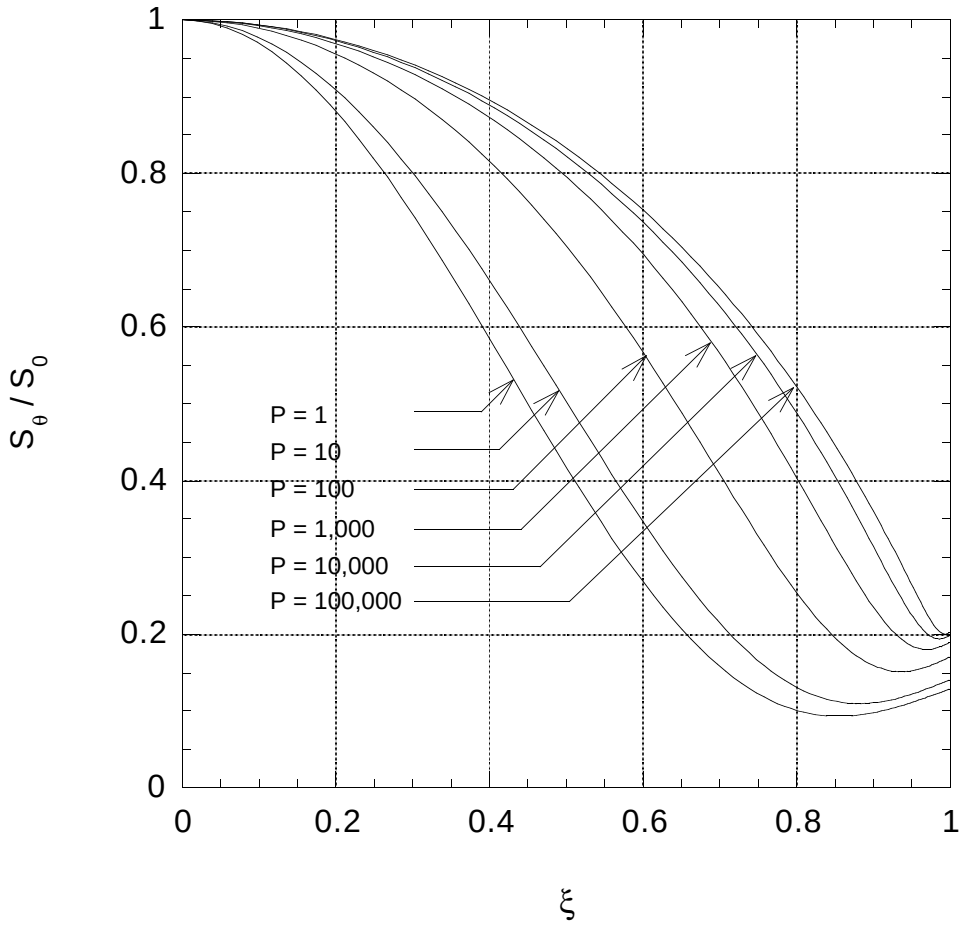

Figure 14: Normalized in-plane tangential stress as a function of radial distance for several values of loading ($k = 0$).

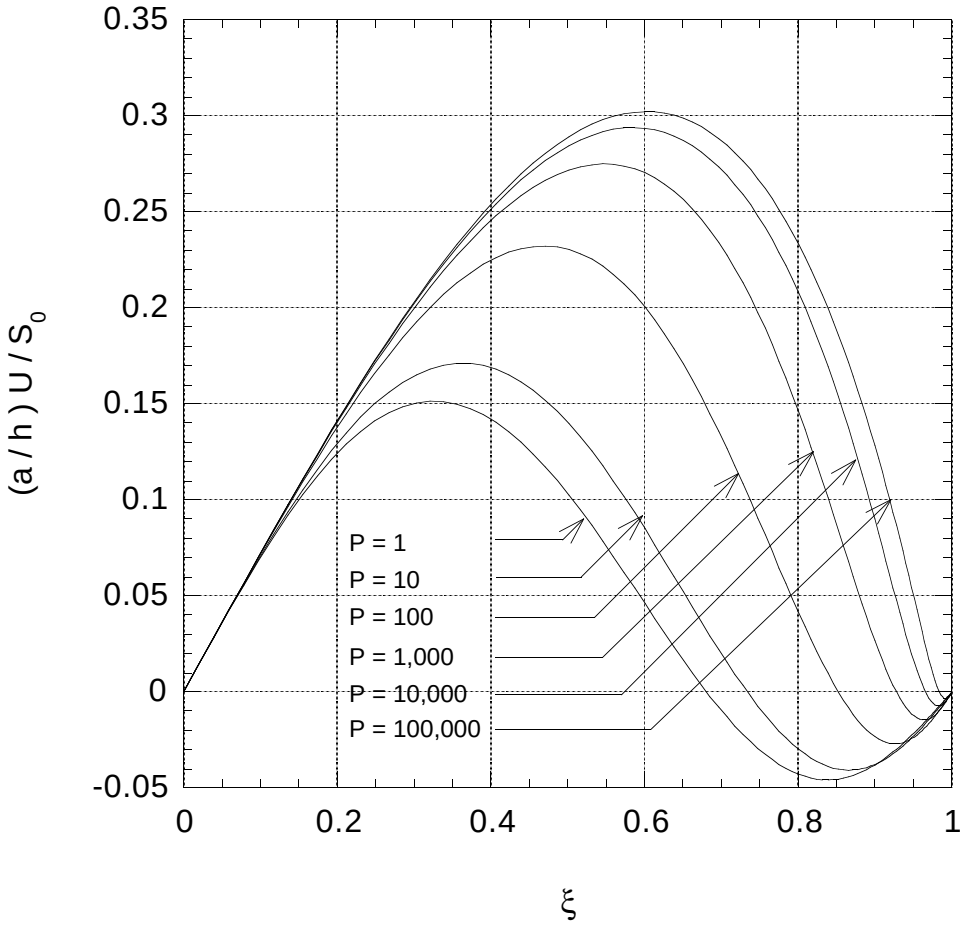

Figure 15: Normalized radial displacement as a function of radial distance for several values of loading ($k = 0$).

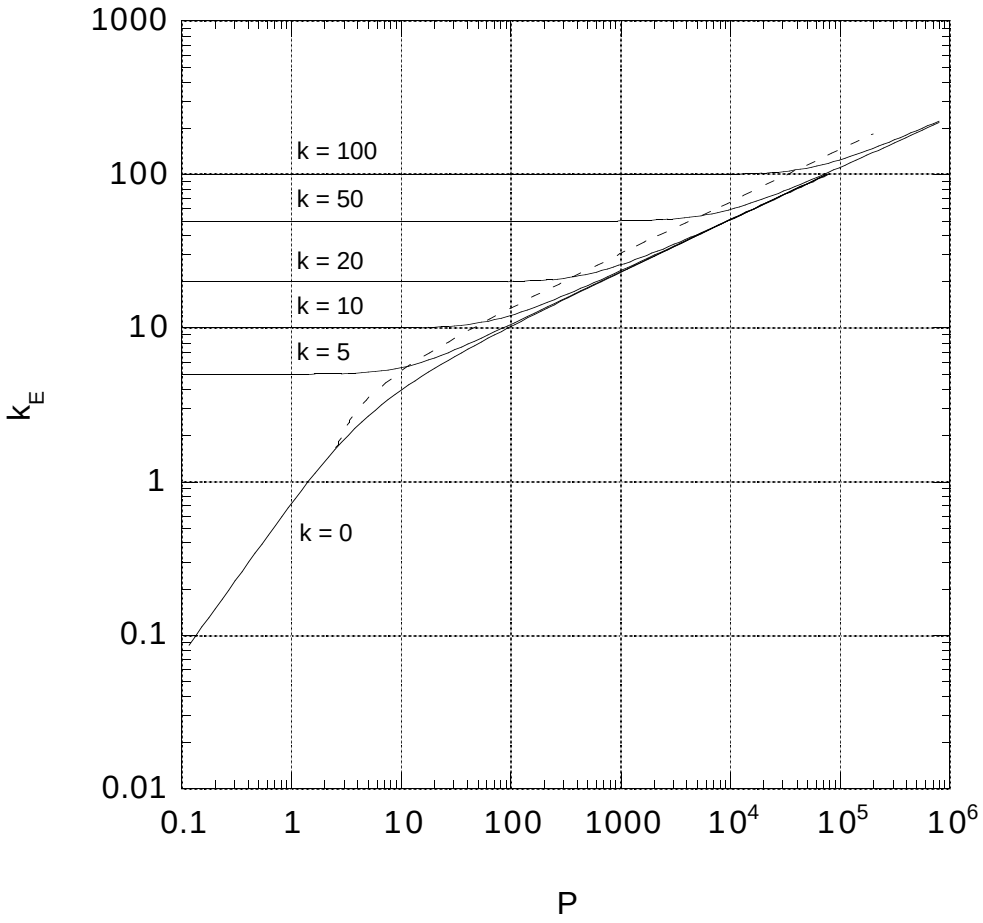

Figure 16: Equivalent tension parameter as a function of loading.